Neuron
Article

Prospective Identification and Purification of Quiescent Adult Neural Stem Cells from Their In Vivo Niche

Paolo Codega,[1,6] Violeta Silva-Vargas,[1,6] Alex Paul,[4,6] Angel R. Maldonado-Soto,[3,6] Annina M. DeLeo,[1,6] Erika Pastrana,[1,9] and Fiona Doetsch[1,2,3,5,6,7,8,*]
[1]Department of Pathology and Cell Biology
[2]Department of Neurology
[3]Department of Neuroscience
[4]Department of Genetics and Development
[5]Department of Rehabilitation and Regenerative Medicine
[6]Columbia Stem Cell Initiative
[7]Motor Neuron Center
[8]Herbert Irving Comprehensive Cancer Center
Columbia University, New York, NY 10032, USA
[9]Present address: Nature Publishing Group, New York, NY 10013, USA
*Correspondence: fkd2101@cumc.columbia.edu
http://dx.doi.org/10.1016/j.neuron.2014.02.039

SUMMARY

Adult neurogenic niches harbor quiescent neural stem cells; however, their in vivo identity has been elusive. Here, we prospectively isolate GFAP$^+$CD133$^+$ (quiescent neural stem cells [qNSCs]) and GFAP$^+$CD133$^+$EGFR$^+$ (activated neural stem cells [aNSCs]) from the adult ventricular-subventricular zone. aNSCs are rapidly cycling, highly neurogenic in vivo, and enriched in colony-forming cells in vitro. In contrast, qNSCs are largely dormant in vivo, generate olfactory bulb interneurons with slower kinetics, and only rarely form colonies in vitro. Moreover, qNSCs are Nestin negative, a marker widely used for neural stem cells. Upon activation, qNSCs upregulate Nestin and EGFR and become highly proliferative. Notably, qNSCs and aNSCs can interconvert in vitro. Transcriptome analysis reveals that qNSCs share features with quiescent stem cells from other organs. Finally, small-molecule screening identified the GPCR ligands, S1P and PGD_2, as factors that actively maintain the quiescent state of qNSCs.

INTRODUCTION

Quiescent and actively dividing (activated) stem cells coexist in adult stem cell niches (Li and Clevers, 2010). Stem cell quiescence and activation play an essential role in many organs, underlying tissue maintenance, regeneration, function, plasticity, aging, and disease. Quiescent stem cells dynamically integrate extrinsic and intrinsic signals to either actively maintain their dormant state or become activated to divide and give rise to differentiated progeny (Cheung and Rando, 2013). To illuminate their biology and their molecular regulation, it is essential to be able to prospectively identify and purify quiescent stem cells. However, this has been exceedingly difficult in any organ, including the adult brain.

Adult neural stem cells (NSCs) continuously generate neurons throughout life in two brain regions: the subgranular zone (SGZ) of the hippocampus and the ventricular-subventricular zone (V-SVZ), adjacent to the lateral ventricles. The V-SVZ is the largest germinal region in the adult mammalian brain and generates olfactory bulb interneurons and oligodendrocytes. Within the V-SVZ, glial fibrillary acidic protein (GFAP)-positive type B cells with hallmark features of astrocytes are stem cells and have multipotent self-renewing capacity in vitro (Doetsch et al., 1999a; Laywell et al., 2000; Imura et al., 2003; Garcia et al., 2004; Sanai et al., 2004; Ahn and Joyner, 2005; Mirzadeh et al., 2008; Beckervordersandforth et al., 2010; Lee et al., 2012). In vivo, actively dividing V-SVZ stem cells are eliminated by antimitotic treatment (Pastrana et al., 2009). In contrast, slowly dividing astrocytes are label-retaining cells (LRCs), survive treatment with antimitotic drugs and regenerate the V-SVZ, and give rise to neurons under homeostasis (Doetsch et al., 1999a; Ahn and Joyner, 2005; Giachino and Taylor, 2009; Nam and Benezra, 2009; Kazanis et al., 2010; Basak et al., 2012).

Recently, novel features of the anatomical organization of the V-SVZ stem cell niche have been uncovered. GFAP$^+$ type B1 cells have a radial morphology and span different compartments of the stem cell niche (Silva-Vargas et al., 2013). Their apical processes contact the lateral ventricle at the center of pinwheel structures formed by ependymal cells, exhibit a primary cilium, and are exposed to signals in the cerebrospinal fluid (CSF) (Doetsch et al., 1999a, Mirzadeh et al., 2008, Beckervordersandforth et al., 2010, Kokovay et al., 2012). Their basal processes contact blood vessels, which are an important proliferative niche in the adult V-SVZ (Shen et al., 2008; Mirzadeh et al., 2008; Tavazoie et al., 2008; Kazanis et al., 2010; Kokovay et al., 2010, Lacar et al., 2011, 2012).

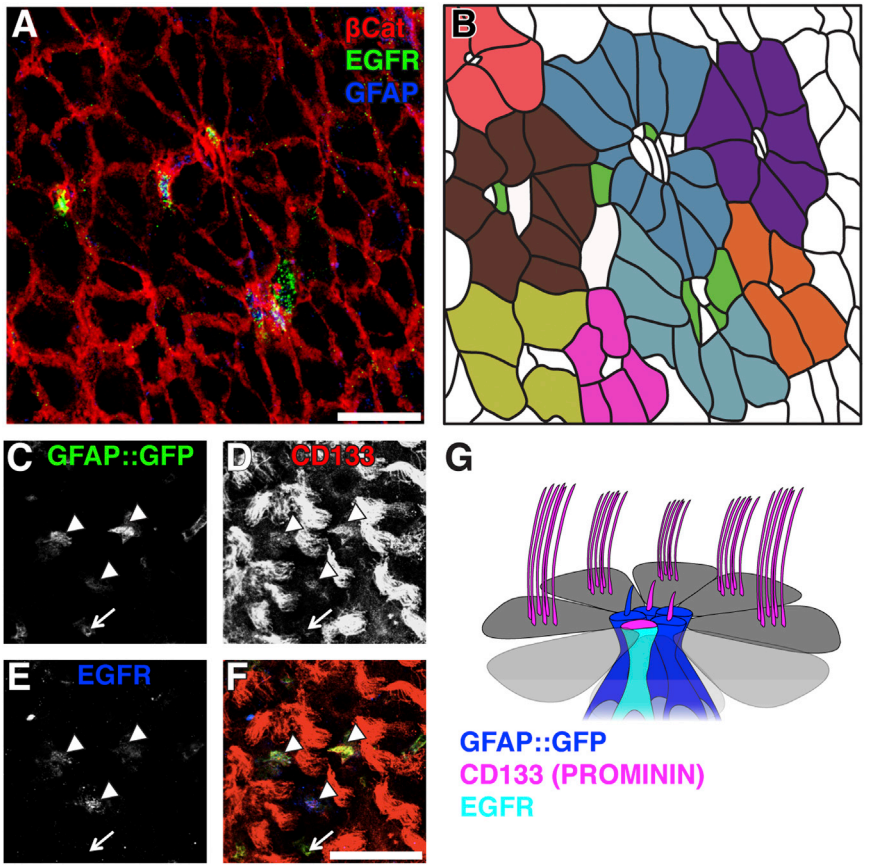

Figure 1. Two Populations of CD133$^+$ V-SVZ Astrocytes Contact the Ventricle

(A and B) A subset of GFAP$^+$ cells at the center of pinwheels express EGFR. (A) Confocal image of a whole mount immunostained for β-catenin ([βCat] red) to visualize pinwheels, GFAP (blue), and EGFR (green). (B) Schematic representation of whole mount shown in (A). Individual pinwheels are highlighted in different colors, and EGFR-expressing cells are green.

(C–F) Optical slice of a confocal z stack at the ventricular surface of a whole mount showing endogenous GFP expression (C) under the control of the human GFAP promoter and immunostained for (D) CD133 and (E) EGFR. (F) Merged image. Note that astrocytes contacting the ventricle with diffuse CD133 staining are EGFR$^+$ (arrowheads), whereas those with CD133 restricted to the primary cilium are EGFR$^-$ (arrow).

(G) Schema showing type B1 astrocytes contacting the ventricle at the center of a pinwheel structure formed by ependymal cells (gray). CD133 (Prominin, magenta) is detected on the cilia of ependymal cells, some primary cilia of some type B1 astrocytes (blue), and is diffusely expressed on the apical surface of EGFR$^+$ type B1 astrocytes (cyan). Scale bars, 30 μm.

See also Figures S1 and S2.

Various molecular markers have been used for the in vivo identification of V-SVZ stem cells and their purification (reviewed in Pastrana et al., 2011). Nestin and Sox2 are widely used as NSC markers in both the embryonic and adult brain (Lendahl et al., 1990; Graham et al., 2003; Kazanis et al., 2010; Imayoshi et al., 2011; Marqués-Torrejón et al., 2013). CD133 (Prominin), a transmembrane glycoprotein expressed on primary cilia of neural progenitors (Uchida et al., 2000; Marzesco et al., 2005; Pinto et al., 2008; Cesetti et al., 2011) has been used to distinguish GFAP$^+$CD133$^+$ stem cells from niche astrocytes (Mirzadeh et al., 2008, Beckervordersandforth et al., 2010). Combinations of markers are beginning to be identified that allow the purification of different subpopulations of V-SVZ cells, in particular of activated stem cells, including epidermal growth factor receptor (EGFR) (Doetsch et al., 2002; Pastrana et al., 2009), and brain lipid binding protein (BLBP) (Giachino et al., 2014). To date, however, combinations of markers have not been identified that allow the prospective isolation of quiescent V-SVZ stem cells. This is crucial to illuminate the functional properties and gene regulatory networks of quiescent adult NSCs.

Herein, we prospectively identify and isolate quiescent adult NSCs from their niche. Our findings reveal that CD133$^+$ astrocytes comprise two functionally distinct populations, quiescent NSCs (qNSCs) and activated NSCs (aNSCs), which differ dramatically in their in vivo cell cycle status and lineage kinetics, their in vitro colony-forming efficiencies, and their molecular signatures. Notably, qNSCs only rarely form colonies in vitro and are natively Nestin negative but upregulate both Nestin and EGFR on activation. qNSCs also share common molecular features with their counterparts in other organs. Finally, we identify GPCR ligands that actively maintain the quiescent state of qNSCs.

RESULTS

Two Populations of CD133$^+$ V-SVZ Astrocytes Contact the Lateral Ventricle

The intermediate filament GFAP is one of the few markers of type B1 astrocytes (Doetsch et al., 1997; Mirzadeh et al., 2008). However, due to its filamentous nature, it is difficult to perform colocalization studies with GFAP, and it cannot be used for live cell sorting. GFAP::GFP mice, in which GFP is expressed under the control of the human GFAP promoter (Zhuo et al., 1997), are a useful tool for visualizing V-SVZ astrocytes in vivo and for their purification by fluorescence-activated cell sorting (FACS) (Tavazoie et al., 2008; Platel et al., 2009, Shen et al., 2008, Pastrana et al., 2009; Beckervordersandforth et al., 2010). Whole-mount preparations allow the pinwheel architecture of the walls of the lateral ventricle to be clearly visualized. We confirmed that, in GFAP::GFP mice, type B1 astrocytes contacting the ventricle at the center of pinwheels were GFP$^+$ and GFAP$^+$, and frequently had a primary cilium, but lacked S100β expression, a marker of mature astrocytes that are found deeper in the tissue at the interface with the striatum (Figures S1A, S1C, and S1D available online).

Notably, a subset of cells localized within individual pinwheels was EGFR$^+$ (11.4% ± 1.3%; n = 129 pinwheels) (Figures 1A and 1B). These ventricle-contacting EGFR$^+$ cells coexpressed

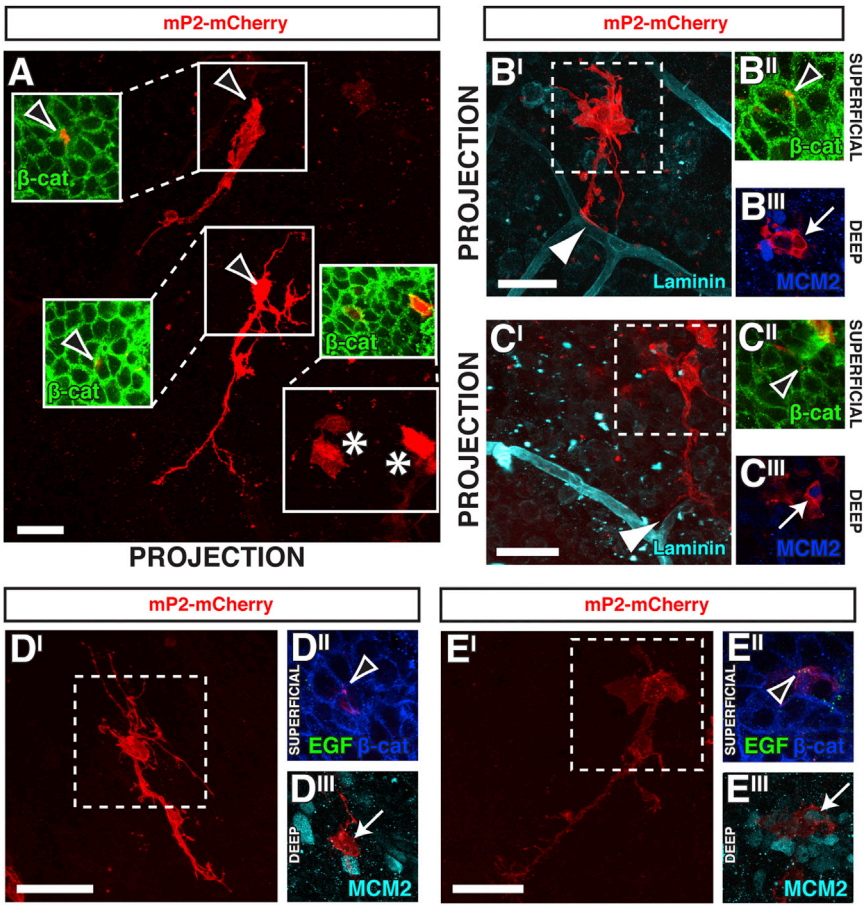

Figure 2. Both Quiescent and Activated CD133$^+$ V-SVZ Astrocytes Have Radial Morphology and Contact the Ventricle and Blood Vessels

(A) Confocal images of whole mounts immunostained with β-catenin ([β-cat] green, superficial optical slice) showing cells labeled by in vivo electroporation of the mP2-mCherry construct (red, z stack projection). Labeled cells are either radial cells that contact the ventricle at the center of pinwheels (open arrowheads in insets) or ependymal cells (asterisks).

(B^I–C^{III}) Confocal images of whole mounts immunostained with Laminin (cyan), β-catenin (green), and MCM2 (blue) showing projections of mP2-mCherry$^+$ cells (B^I and C^I). Insets show superficial (B^{II} and C^{II}) and deep (B^{III} and C^{III}) optical slices. Both MCM2$^-$ and MCM2$^+$ cells contact the ventricle at the center of pinwheels as well as blood vessels.

(D^I–E^{III}) Confocal images of whole mounts immunostained with MCM2 (cyan) and β-catenin (blue) and labeled with EGF-A647 (green) showing projections of mP2-mCherry$^+$ cells (D^I and E^I). Insets show superficial (D^{II} and E^{II}) and deep (D^{III} and E^{III}) optical slices. Note that EGF-negative cells are MCM2$^-$. Scale bars, 30 μm.

See also Figure S3.

both GFAP protein and GFP in GFAP::GFP mice (Figure S1B; Pastrana et al., 2009) and were observed throughout the rostrocaudal axis of the V-SVZ, with 45.7% ± 4.4% of pinwheels containing EGFR$^+$ cells.

To define markers for EGFR-negative type B1 cells contacting the ventricle, we examined the expression of CD133 (Prominin), which is expressed by ependymal cells and on the primary cilium of some type B1 cells (Coskun et al., 2008; Mirzadeh et al., 2008; Beckervordersandforth et al., 2010). We immunostained whole mounts of GFAP::GFP mice for EGFR and CD133 in conjunction with β-catenin (to label pinwheels) or acetylated tubulin (to detect primary cilia). We thereby identified two CD133$^+$ astrocyte populations: GFAP::GFP$^+$CD133$^+$ and GFAP::GFP$^+$CD133$^+$EGFR$^+$ (Figure 1G). GFAP::GFP$^+$CD133$^+$ cells had a primary cilium with CD133 staining localized to its tip (Figures 1C–1F; Figures S2A and S2C). In contrast, GFAP::GFP$^+$CD133$^+$EGFR$^+$ cells exhibited diffuse CD133 staining over their apical surface and lacked a primary cilium (Figures 1C–1F; Figures S2B and S2D). Finally, we also observed GFAP::GFP$^+$ cells contacting the ventricle, which had a primary cilium that was CD133 negative (Figures S2A and S2C).

Visualizing the in vivo morphology of CD133$^+$ type B1 cells is not feasible by immunostaining. To this end, we cloned and electroporated a construct that expresses membrane-targeted mCherry under the control of the mouse minimal P2 (Prominin-1) promoter (mP2-mCherry; Figure S3A) into the lateral ventricle and analyzed whole mounts 2 days later. Both multiciliated flat ependymal cells possessing typical cuboidal morphology and radial cells with B1 morphology were labeled by this construct (Figure 2A), and all coexpressed CD133 protein (23/23 cells; Figures S3B–S3D). Radial mP2-mCherry$^+$ cells expressed CD133 either at the tip of their primary cilium (Figure S3C) or diffusely on their apical surface (Figure S3D) and were GFAP$^+$ (data not shown). To define the cell cycle status and relationship of radial mP2-mCherry$^+$ cells with ependymal cells and blood vessels, electroporated whole mounts were immunostained for combinations of EGF-A647, MCM2, β-catenin, and Laminin to label activated stem cells, dividing cells, pinwheels, and blood vessels, respectively. All radial mP2-mCherry$^+$ cells, regardless of MCM2 expression or epidermal growth factor (EGF)-ligand binding, had a typical B1 morphology with an apical process contacting the ventricle at the center of pinwheels and a long basal process extending away from the surface, which frequently terminated on blood vessels (Figures 2B^I–2B^{III}; Figures 2C^I–2C^{III}; Figures S3E–S3N). Importantly, all MCM2$^+$ radial mP2-mCherry$^+$ astrocytes were colabeled with EGF-ligand (70/70 cells MCM2$^-$ and EGF$^-$; 5/5 cells MCM2$^+$ and EGF$^+$; Figures 2D^I–2D^{III}; Figures 2E^I–2E^{III}).

Prospective Purification of V-SVZ Astrocytes

The aforementioned in vivo characterization suggests that CD133 and EGFR could be used as markers to prospectively purify quiescent and activated NSCs directly from their in vivo

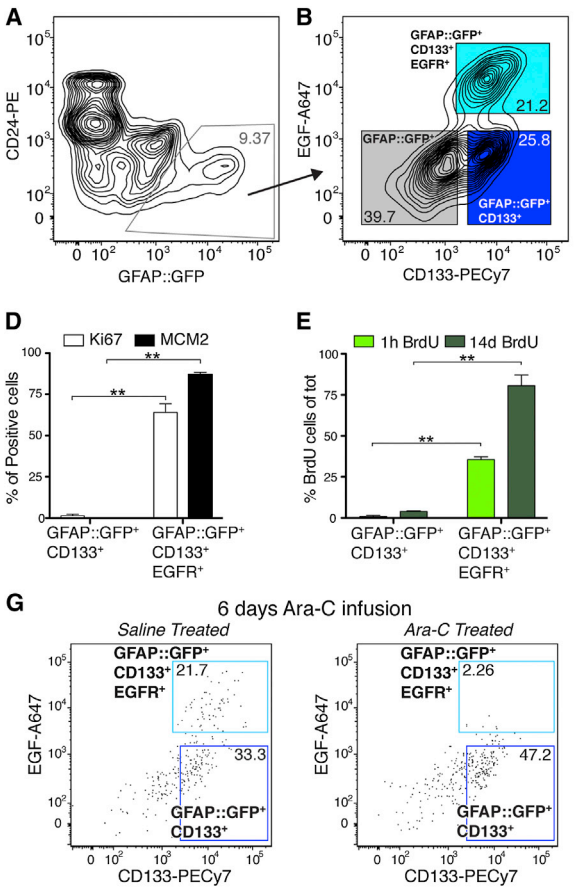

Figure 3. Prospectively Purified CD133⁺ Astrocyte Subpopulations Exhibit Different Cell Cycle Properties

(A and B) Representative FACS plots showing gating strategy. In (A), the gate used to select GFAP::GFP⁺CD24⁻ cells, which are then gated on EGF-A647 and CD133-PE-Cy7. In (B), three populations are clearly defined: GFAP::GFP⁺ (gray), GFAP::GFP⁺CD133⁺ (blue), and GFAP::GFP⁺CD133⁺EGFR⁺ (cyan).

(C) Histogram showing the intensity of GFP signal in GFAP::GFP⁺, GFAP::GFP⁺CD133⁺, and GFAP::GFP⁺CD133⁺EGFR⁺ populations (gray, blue, and cyan, respectively) compared to other V-SVZ cells (GFP⁻, black). Note that GFAP::GFP⁺CD133⁺EGFR⁺ cells are dimmer than GFAP::GFP⁺ and GFAP::GFP⁺CD133⁺ cells.

(D) Proportion of each CD133⁺-purified astrocyte subpopulation that expresses Ki67 and MCM2 ($n = 3$; $^{**}p < 0.01$, unpaired Student's t test; mean ± SEM).

(E) Proportion of each CD133⁺-purified astrocyte subpopulation labeled after a single pulse of BrdU (light green) or after 14 days of BrdU in the drinking water (dark green) ($n = 3$ and $n = 4$, respectively, $^{**}p < 0.01$, unpaired Student's t test, mean ± SEM).

(F) LRC fraction in the CD133⁺-purified astrocyte populations 14 or 30 days after 14 days of BrdU administration ($n = 4$, mean ± SEM).

(G) Representative FACS plots of CD133⁺ astrocyte subpopulations from saline- and Ara-C-treated mice.

(H) Summary of markers expressed by CD133⁺-purified astrocytes.

See also Figures S4 and S6.

niche using FACS. We previously developed a simple strategy to simultaneously isolate activated stem cells (GFAP::GFP⁺EGFR⁺), transit-amplifying cells (EGFR⁺), and neuroblasts (CD24⁺) by combining EGF-A647 and CD24 in GFAP::GFP mice (Pastrana et al., 2009). By including CD133 in this sorting strategy, we separated two CD133⁺ astrocyte populations, GFAP::GFP⁺CD133⁺ and GFAP::GFP⁺CD133⁺EGFR⁺, from the remaining GFAP::GFP⁺-only cells (Figures 3A and 3B; Figures S4A–S4I). GFAP::GFP⁺CD133⁺ (ranging from 25% to 30% of total GFP⁺ cells) and GFAP::GFP⁺CD133⁺EGFR⁺ (20%–25% of total GFP⁺ cells) were both abundant but differed in their GFP brightness (Figure 3C).

We assessed the purity of the sorted populations using qRT-PCR and acute immunostaining. qRT-PCR confirmed that sorted populations were appropriately enriched in *Gfap*, *GFP*, *Prom1*, and *Egfr* expression (Figures S4Q–S4T). Acute immunostaining showed that both GFAP::GFP⁺CD133⁺ and GFAP::GFP⁺CD133⁺EGFR⁺ populations were highly enriched in GLAST and GLT1 (Figures S4J and S4K)—glutamate aspartate transporters expressed in astrocytes—as well as BLBP (Figure S4M), that they largely or completely lacked S100β (Figure S4L) and that they were almost completely negative for the neuroblast markers DCX and βIII tubulin (Figures S4O and S4P). Notably, more than 90% of GFAP::GFP⁺CD133⁺ and GFAP::GFP⁺CD133⁺EGFR⁺ populations expressed the NSC transcription factor Sox2 (Figures S4N and S4U). High Sox2 levels are related to a more proliferative state (Marqués-Torrejón et al., 2013); of note, 92.8% ± 1.5% of GFAP::GFP⁺CD133⁺EGFR⁺ cells expressed high levels of Sox2 protein, whereas only 38.4% ± 3.5% of GFAP::GFP⁺CD133⁺ cells were Sox2 bright, with the remainder being Sox2 dim. In contrast, the GFAP::GFP⁺-only population was more heterogeneous with significant neuroblast contamination, likely due to perdurance of GFP in neuroblasts (Figures S4O and S4P). We therefore focused our functional analyses below on GFAP::GFP⁺CD133⁺ and GFAP::GFP⁺CD133⁺EGFR⁺ populations (all data regarding the GFAP::GFP⁺-only population are included in Figure S6).

Purified GFAP⁺CD133⁺ V-SVZ Cells Have Different Cell Cycle Properties

Quiescent stem cells are largely dormant and lack markers of proliferation such as Ki67 and MCM2 that are expressed in actively dividing cells, but not during the quiescent G_0 state (Maslov et al., 2004). Both markers are expressed during G_1, with MCM2 being expressed earlier than Ki67. Cycling GFAP⁺ V-SVZ cells in vivo have a fast cell cycle (Ponti et al., 2013). To determine the cell cycle properties of CD133⁺ astrocyte subpopulations in vivo, we used multiple approaches. First, we determined the instantaneous cell cycle status of FACS-purified cells by acute immunostaining for proliferation-associated markers. GFAP::GFP⁺CD133⁺EGFR⁺ cells were highly enriched in both Ki67 and MCM2 (64% ± 5.2% and 87.3% ± 1.2%,

respectively) whereas these two markers were almost absent in GFAP::GFP$^+$CD133$^+$ cells (1.4% ± 0.9% and 0.0% ± 0.0%, respectively) (Figure 3D). Similar patterns of proliferation were observed after a single in vivo pulse of bromodeoxyuridine (BrdU) 1 hr prior to FACS isolation: 35.5% ± 1.8% of GFAP::GFP$^+$CD133$^+$EGFR$^+$ cells were BrdU$^+$, in contrast to 0.8% ± 0.8% of GFAP::GFP$^+$CD133$^+$ cells (Figure 3E). Thus, at any given moment, the vast majority of GFAP::GFP$^+$CD133$^+$ cells are not proliferating.

LRCs are slowly cycling cells whose DNA remains labeled after prolonged administration of thymidine analogs and a long chase period (Wilson et al., 2008). To label dividing cells and to identify LRCs, we administered BrdU via drinking water for 2 weeks and analyzed the proportion of each population that was BrdU$^+$. Immediately after BrdU treatment, almost all GFAP::GFP$^+$CD133$^+$EGFR$^+$ cells were labeled, whereas only 3.9% ± 0.4% of GFAP::GFP$^+$CD133$^+$ cells had incorporated BrdU, reflecting their much slower rate of division (Figure 3E). Fourteen days after ceasing BrdU treatment, GFAP::GFP$^+$CD133$^+$EGFR$^+$ cells had already almost completely lost BrdU labeling (Figure 3F). In contrast, 52.4% ± 17.3% of GFAP::GFP$^+$CD133$^+$ cells were still BrdU$^+$ 30 days after BrdU withdrawal (Figure 3F).

Finally, we confirmed the different proliferation characteristics of both populations in vivo by infusing cytosine-β-D-arabinofuranoside (Ara-C) directly on the brain surface to eliminate dividing cells (Doetsch et al., 1999b). GFAP::GFP$^+$CD133$^+$ cells survived 6 days of Ara-C treatment, whereas the more rapidly dividing GFAP::GFP$^+$CD133$^+$EGFR$^+$ cells were eliminated (Figure 3G). Thus, although CD133 is regulated in a cell-cycle-dependent manner in dividing neural cell lines (Sun et al., 2009), in the V-SVZ niche, CD133 is expressed in both dividing and nondividing cells in vivo.

Together, these findings reveal that GFAP::GFP$^+$CD133$^+$ cells are largely quiescent in vivo, whereas GFAP::GFP$^+$CD133$^+$EGFR$^+$ cells are actively dividing. Based on their cell cycle properties and the functional studies described below, hereafter we refer to these populations as qNSCs and aNSCs, respectively (Figure 3H).

qNSCs and aNSCs Are Both Neurogenic In Vivo but Differ in Their Kinetics

To assess the in vivo potential of quiescent and activated stem cells, we transplanted purified qNSCs (1 week, n = 8; 1 month, n = 5) and aNSCs (1 week, n = 5; 1 month, n = 11) isolated from GFAP::GFP;β-Actin-PLAP mice (Zhuo et al., 1997; DePrimo et al., 1996) into the SVZ of wild-type recipient mice (Figure 4A). The donor cells were histochemically visualized based on their expression of the reporter human placental alkaline phosphatase (PLAP). In mice transplanted with aNSCs, many migrating neuroblasts were present in the V-SVZ, the rostral migratory stream (RMS), and the olfactory bulb after only 1 week (Figures 4E–4G), confirming their activated state. However, in mice transplanted with qNSCs, no neuroblasts were observed at this time point, and PLAP$^+$ cells were only present in the V-SVZ (Figures 4B–4D). In contrast, after 1 month, both populations generated mature olfactory bulb interneurons (Figures 4J and 4M), and PLAP$^+$ cells were still present in the V-SVZ in all transplants (Figures 4H and 4K). Interestingly, migrating neuroblasts were also present in the RMS in 3 out of 5 qNSC and 3 out of 11 aNSC transplanted brains, demonstrating that both populations continue to generate neurons after 1 month in vivo (Figures 4I and 4L). Oligodendrocytes were also formed by both transplanted populations (data not shown). These data show that both qNSCs and aNSCs can give rise to neurons and retain long-term neurogenic potential in vivo but exhibit very different kinetics of cell generation.

qNSCs and aNSCs Differ in Their In Vitro Behavior and Can Interconvert States

Two in vitro assays are widely used to assess stem cell properties and to enumerate in vivo stem cells: adherent colony formation and neurospheres (Pastrana et al., 2011). With the ability to now prospectively purify qNSCs, we directly tested their in vitro behavior in both assays, as compared to aNSCs.

qNSCs and aNSCs were plated as single cells under adherent conditions in the presence of EGF or EGF/basic fibroblast growth factor (bFGF). Whereas aNSCs were enriched in colony formation (47.9% ± 11.9% in EGF and 41.4% ± 1.8% in EGF/bFGF), in striking contrast, qNSCs only rarely gave rise to colonies (1.2% ± 0.1% in EGF and 0.7% ± 0.2% in EGF/bFGF) (Figure 5A) and did so with much slower growth kinetics than aNSCs. Importantly, although rare, the colonies formed by single qNSCs were large and multipotent, giving rise to neurons, oligodendrocytes, and mature astrocytes (Figures 5B and 5C).

We next compared the ability of qNSCs and aNSCs to form neurospheres and assessed self-renewal by serial passaging. Again, qNSCs only rarely gave rise to neurospheres (0.85% in EGF, 0.82% in EGF/bFGF) in contrast to aNSCs, which robustly generated neurospheres (Figure S5B). Moreover, the proliferation of the qNSC population was delayed by 6 days compared to aNSCs (Figures 5D and S5A). However, once activated, qNSCs exhibited similar rates of division to aNSCs. Neurospheres from both populations could be serially passaged more than three times and were multipotent, giving rise to neurons, astrocytes, and oligodendrocytes (Figures S5B and S5E). Finally, we examined whether more qNSCs were recruited to form neurospheres during in vivo regeneration, at 12 hr post-Ara-C removal when stem cell astrocytes start to divide (Doetsch et al., 1999a, 1999b; Pastrana et al., 2009). Notably, the efficiency of neurosphere formation of qNSCs purified after Ara-C treatment did not increase (Figure 5K). However, as previously shown, total neurosphere formation was almost completely eliminated after Ara-C treatment (Doetsch et al., 2002; Imura et al., 2003; Morshead et al., 2003; Garcia et al., 2004; data not shown), confirming that the vast majority of neurospheres arise from actively dividing cells.

Together, these results reveal that aNSCs are highly enriched in colony formation. In contrast, the qNSC population rarely forms colonies and does so more slowly than aNSCs. However, once activated, qNSCs are highly proliferative and multipotent, almost indistinguishable from aNSCs (Figure S5B). We therefore assessed whether qNSCs and aNSCs can interconvert in vitro by dissociating and analyzing primary spheres by flow cytometry. Intriguingly, the vast majority of cells in neurospheres derived from qNSCs expressed both EGFR and CD133 (Figures 5E

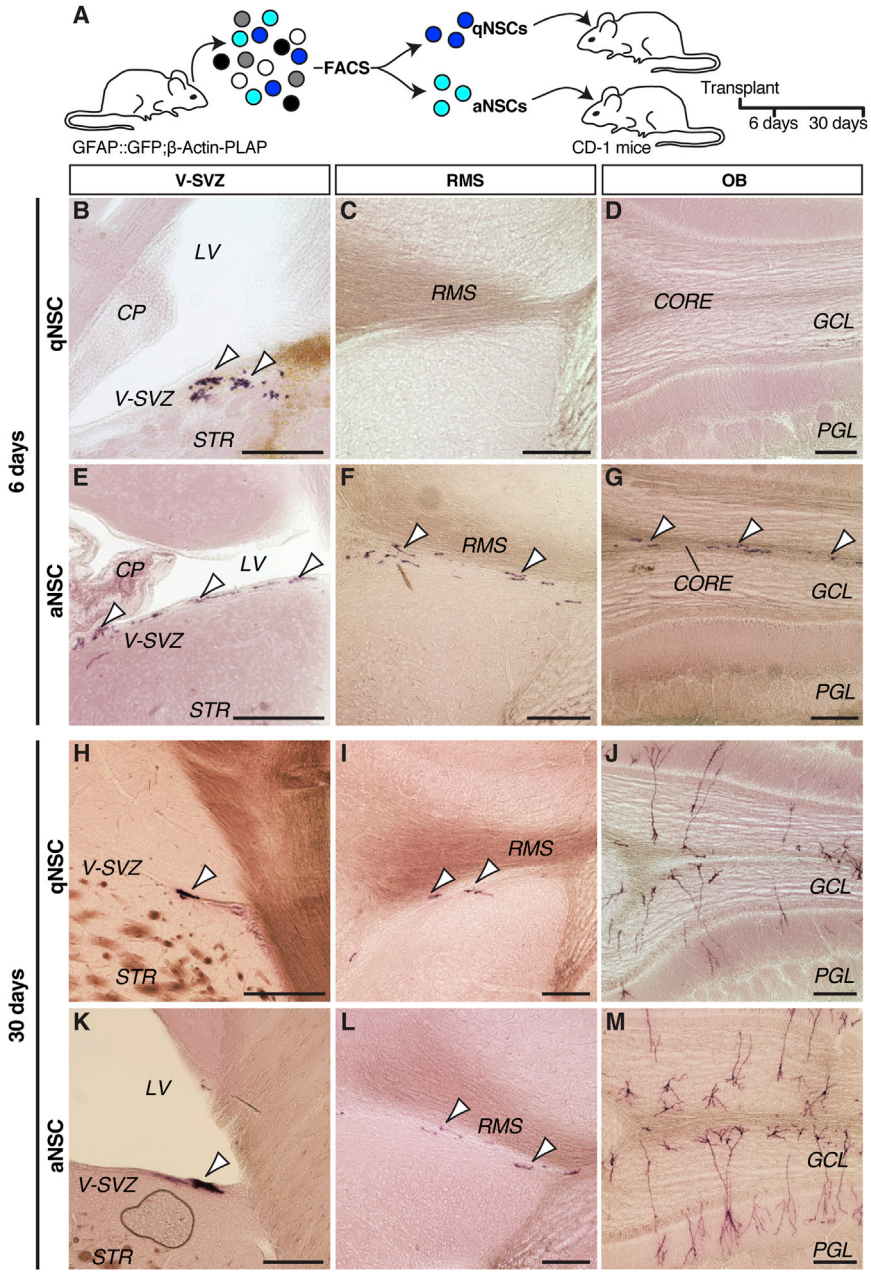

Figure 4. qNSCs and aNSCs Are Neurogenic In Vivo

(A) Schema of experimental design.

(B–G) Horizontal brain sections showing PLAP$^+$ cells (purple, arrowheads) 1 week after transplantation of qNSCs (B–D) and aNSCs (E–G). At this time point, aNSCs generated numerous migrating neuroblasts, whereas no cells were detected in the RMS or in the olfactory bulb of brains transplanted with qNSCs.

(H–M) Horizontal brain sections showing PLAP$^+$ cells (purple, arrowheads) 1 month after transplantation of (H–J) qNSCs and (K–M) aNSCs. In transplants from both populations, cells were present in the V-SVZ and RMS and had generated mature olfactory bulb interneurons. Scale bars, 200 μm. STR, striatum; CP, choroid plexus; LV, lateral ventricle; GCL, granular cell layer; PGL, periglomerular layer.

and 5G), revealing that qNSCs give rise to GFAP::GFP$^+$CD133$^+$EGFR$^+$ cells in vitro. Conversely, aNSCs gave rise to both GFAP::GFP$^+$CD133$^+$ and GFAP::GFP$^+$ populations (Figures 5F and 5H). Moreover, when primary spheres were dissociated and GFAP::GFP$^+$CD133$^+$, GFAP::GFP$^+$CD133$^+$EGFR$^+$, and GFAP::GFP$^+$ cells were reisolated, each population exhibited similar sphere formation efficiencies to primary isolated cells, with the GFAP::GFP$^+$CD133$^+$EGFR$^+$ population being greatly enriched in neurosphere formation compared to GFAP::GFP$^+$CD133$^+$ and GFAP::GFP$^+$ populations (Figures 5I and 5J; Figures S5C and S5D). Therefore, qNSCs and aNSCs can interconvert between more quiescent and activated states, with each population giving rise to all other populations in vitro.

qNSCs Do Not Express Nestin but Upregulate EGFR and Nestin on Activation

Nestin is an intermediate filament protein; its expression is widely considered a hallmark of NSCs, both during development and in the adult (Lendahl et al., 1990; Imayoshi et al., 2011). Unexpectedly, our microarray analysis (see below) suggested that qNSCs express very low to no levels of Nestin mRNA, in contrast to aNSCs, in which Nestin mRNA is highly expressed. We confirmed this observation by qRT-PCR (Figure S8E) as well as by immunostaining of acutely purified cells (Figure 6A). Out of 1,582 plated qNSCs, none were Nestin protein positive. Finally, to assess the Nestin status of NSCs in vivo, we electroporated mice with the mP2-mCherry construct and coimmunostained whole mounts with Nestin and EGF-ligand. In vivo, Nestin is highly expressed by ependymal cells (Doetsch et al., 1997; Figures 6D^{I} and 6E^{I}) as well as SVZ cells (Figures 6D^{II} and 6E^{II}). All radial EGF-ligand-negative mP2-mCherry$^+$ cells were Nestin protein negative (Figures 6D^{I} and 6D^{II}; 0/79 cells in seven whole mounts). In contrast, only EGF-ligand-positive cells coexpressed Nestin protein (Figures 6E^{I} and 6E^{II}; 32/34 cells in seven whole mounts).

To investigate whether qNSCs upregulate Nestin protein on activation, we performed a time-course analysis of qNSCs cultured in adherent conditions and immunostained for Nestin, EGFR, and MCM2 (Figures 6B and 6C). When first isolated and plated, qNSCs were small and round and did not express Nestin, EGFR, or MCM2 (type 1). As qNSCs became activated in vitro, they underwent morphological and molecular changes, enlarging their nuclei and upregulating all three markers

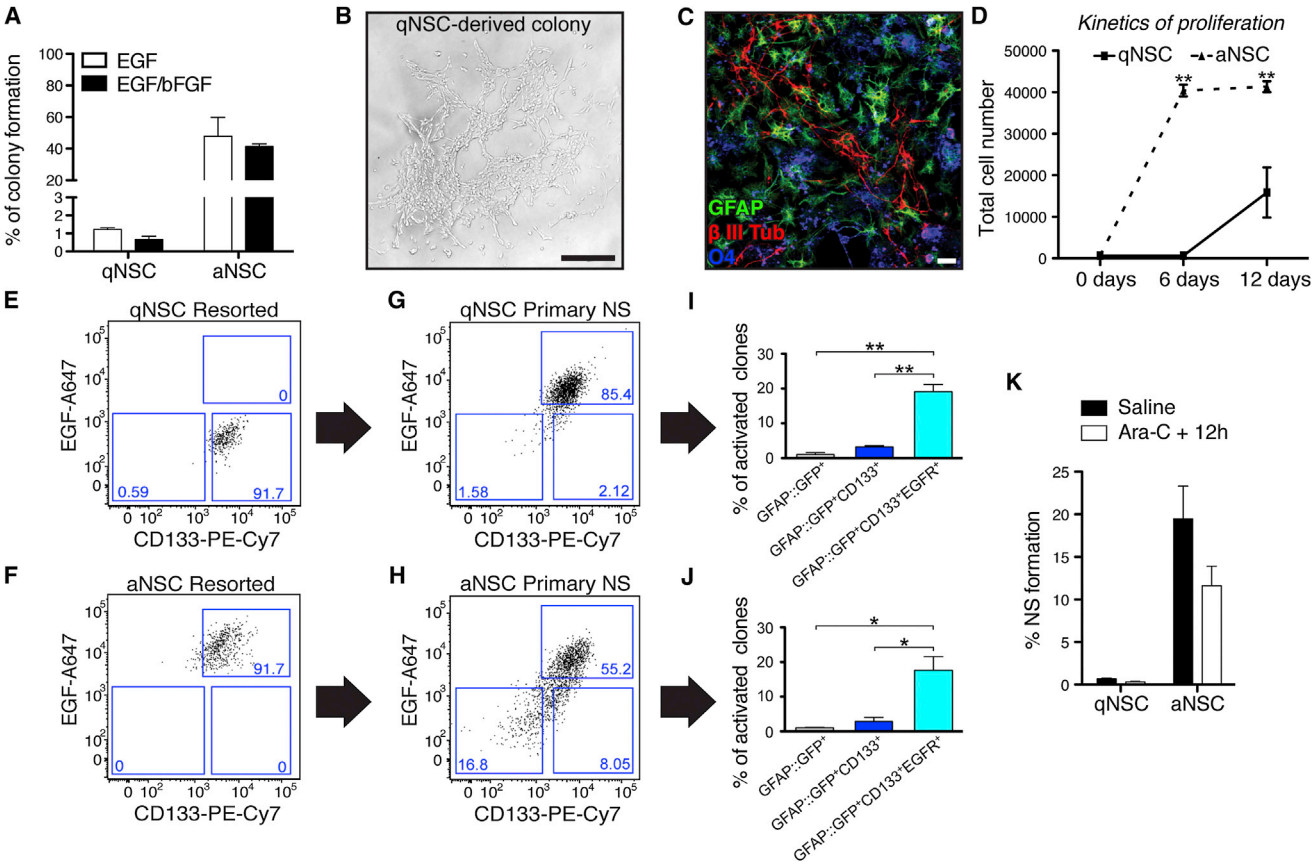

Figure 5. Purified qNSCs and aNSCs Give Rise to Neurospheres with Different Proliferative Properties and Kinetics

(A) Single cell colony formation efficiency of FACS-purified qNSCs and aNSCs in adherent cultures (n = 3, mean ± SEM).

(B) Representative phase contrast image of an adherent colony from a single qNSC after 12 days in the presence of EGF. Scale bar, 100 μm.

(C) Confocal image of neurons (βIII Tubulin [β III Tub], red), astrocytes (GFAP, green) and oligodendrocytes (O4, blue) derived from qNSCs plated under adherent conditions. Scale bar, 10 μm.

(D) Quantification of cell proliferation when plated at 1.4 cells per microliter with EGF under nonadherent conditions after 6 or 12 days (n = 5; **p < 0.01 compared to qNSCs at the same time point, unpaired Student's t test, mean ± SEM).

(E–H) Representative FACS plots of, in (E) and (F), purified $CD133^+$ astrocytes immediately resorted after isolation from the brain and, in (G) and (H), of primary neurospheres (NS) derived from each population after 12 days for qNSCs and 6 days for aNSCs cultured in EGF.

(I and J) Clonal activation efficiency of purified $GFAP::GFP^+$, $GFAP::GFP^+CD133^+$, and $GFAP::GFP^+CD133^+EGFR^+$ cells, isolated from primary neurospheres of each population (in EGF, n = 3; *p < 0.05, **p < 0.01, unpaired Student's t test; mean ± SEM).

(K) Neurosphere formation 12 hr (12h) after Ara-C treatment as compared to saline-treated controls (n = 6, mean ± SEM).

See also Figures S5 and S6.

(type 2). They then extended processes (type 3) (Figures 6B and 6C) and began to proliferate extensively, closely resembling cultured aNSCs.

To independently confirm the lack of Nestin expression in qNSCs and its upregulation on activation, we used Nestin::Kusabira Orange reporter mice (Kanki et al., 2010; Ishizuka et al., 2011) to FACS-purify $CD133^+Nes::OR^-EGFR^-CD24^-$ (Nestin- and EGFR-negative) cells (Figure S7A). Acutely plated cells all lacked Nestin protein (Figure S7B) and, when cultured, only rarely gave rise to neurospheres (Figures S7C and S7E). Importantly, $CD133^+Nes::OR^-EGFR^-CD24^-$ cells, which originally lacked Nestin::Kusabira Orange reporter expression, upregulated the reporter in all neurospheres that formed (Figure S7C). In contrast, purified $CD133^+Nes::OR^+EGFR^+CD24^-$ cells were very efficient in neurosphere formation (Figures S7D and S7E).

Finally, we examined whether Nestin-negative qNSCs contribute to the lineage during regeneration. At present, it is not feasible to directly trace the lineage of qNSCs in vivo due to the lack of specific markers. We therefore administered tamoxifen to adult GFAP::CreERT2;$Rosa26^{tdTomato}$ mice to induce recombination in GFAP-expressing cells and chased for 10 days after the first injection to allow actively dividing cells to progress down the lineage (Figure S7F). We then infused Ara-C for 6 days to eliminate dividing cells (Figure S7F) and confirmed that all remaining lineage-labeled cells were Nestin negative (0 of 951; Figure S7G) immediately after termination of treatment. Six days after Ara-C removal, $tdTomato^+Nestin^+$ cells were present (Figures S7H and S7I), as well as $tdTomato^+DCX^+$ neuroblasts (Figure S7I). These data reveal that qNSCs upregulate Nestin, as well as EGFR, during

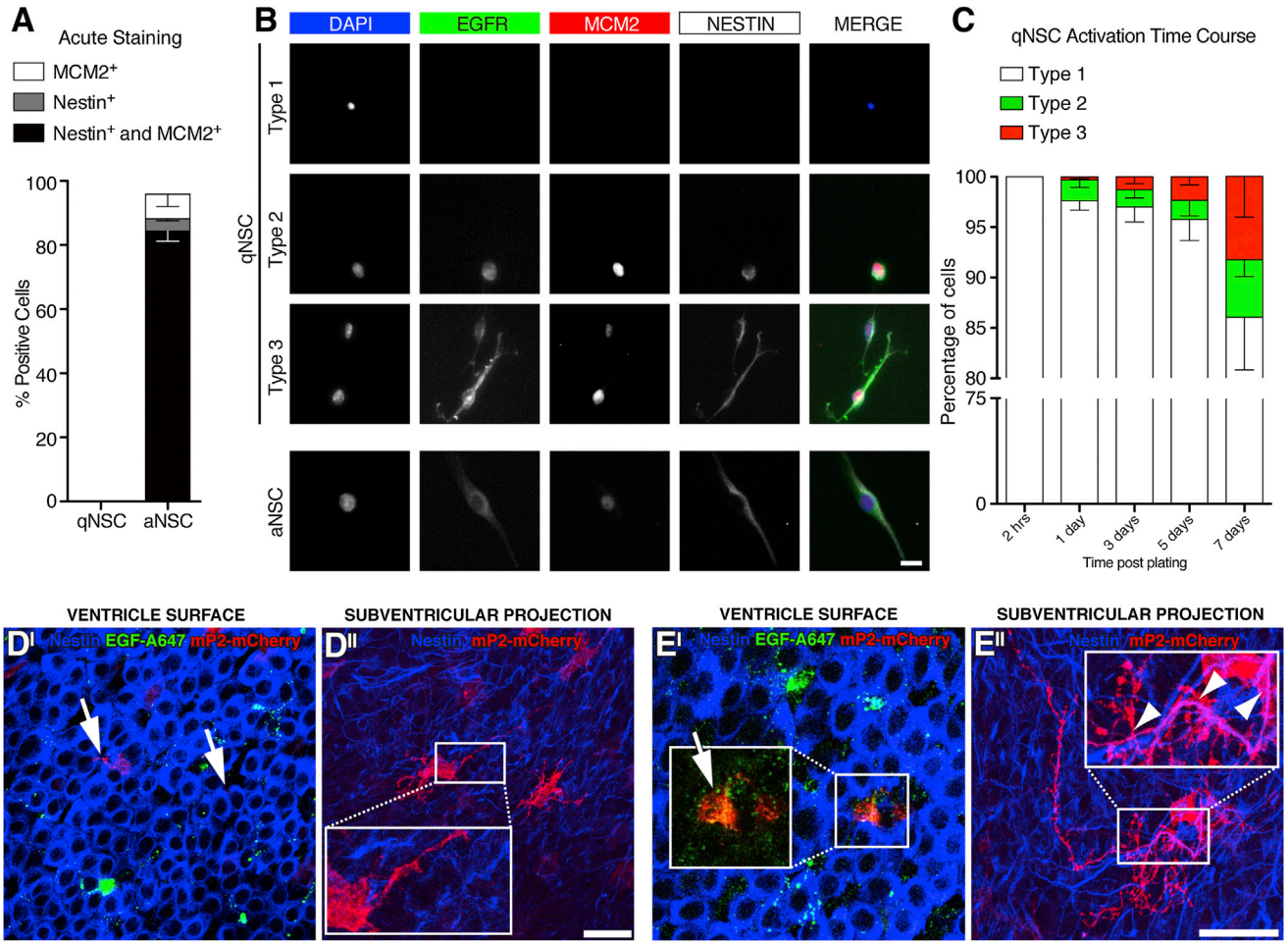

Figure 6. qNSCs Are Nestin Negative

(A) Proportion of acutely plated purified qNSCs and aNSCs immunopositive for MCM2 and Nestin (n = 3, mean ± SEM).

(B) Images of FACS-purified qNSCs cultured in EGF, fixed at different time points, and immunostained with EGFR, MCM2, and Nestin. Three types of cells are present: rounded cells with a condensed nucleus that do not express EGFR, MCM2, or Nestin (type 1); rounded cells with a larger nucleus that express EGFR, MCM2, and Nestin (type 2); and EGFR$^+$MCM2$^+$Nestin$^+$ cells with elongated processes (type 3). Type 3 cells resemble aNSCs after 3 days in culture. Scale bars, 10 μm.

(C) Quantification of activated qNSCs in culture after 2 hr or after 1, 3, 5, or 7 days after plating (n = 4, mean ± SEM).

(D^I–E^{II}) Confocal images showing mP2-mCherry$^+$ cells (red) in whole mount labeled with EGF-A647 (green) and immunostained for Nestin (blue). In (D), two cells contact the ventricle between ependymal cells, do not bind EGF-A647 (D^I, arrows), and are Nestin negative in the subventricular projection (D^{II}). In (E), an EGF-A647-labeled cell (E^I, arrow) is coimmunostained with Nestin in the subventricular projection (E^{II}, arrowheads in inset). Notably, not all processes contained Nestin. Scale bars, 30 μm.

See also Figure S7.

activation and contribute to the lineage during regeneration in vivo.

Gene Expression Analysis of Purified qNSCs and aNSCs Reveals Distinct Molecular Signatures

To gain insight into the biological properties of qNSCs and to define their molecular signatures, we performed microarray analysis on RNA from FACS-purified populations isolated directly from their in vivo niche (Figure 7A; Table S1). Gene ontology (GO) and gene set enrichment analysis (GSEA) (Subramanian et al., 2005) revealed that qNSCs and aNSCs have distinct molecular features (Figures 7B–7D). Confirming the actively dividing state of aNSCs in vivo, their transcriptome was enriched in genes involved in the cell cycle, transcription and translation, and DNA repair (Figures 7C and 7D; Tables S2 and S3). In contrast, qNSCs were enriched in the GO categories of cell communication, response to stimulus, and cell adhesion (Figure 7B; Table S2), underscoring the dynamic regulation of the quiescent state via interaction with the microenvironment. Indeed, the most represented GSEA groups for qNSCs were related to transport, signaling, receptors, cell surface, and extracellular matrix (Figure 7D; Table S3). Notably, qNSCs and aNSCs exhibited different metabolic profiles; the majority of the differentially enriched GSEA metabolism subsets in qNSCs were related

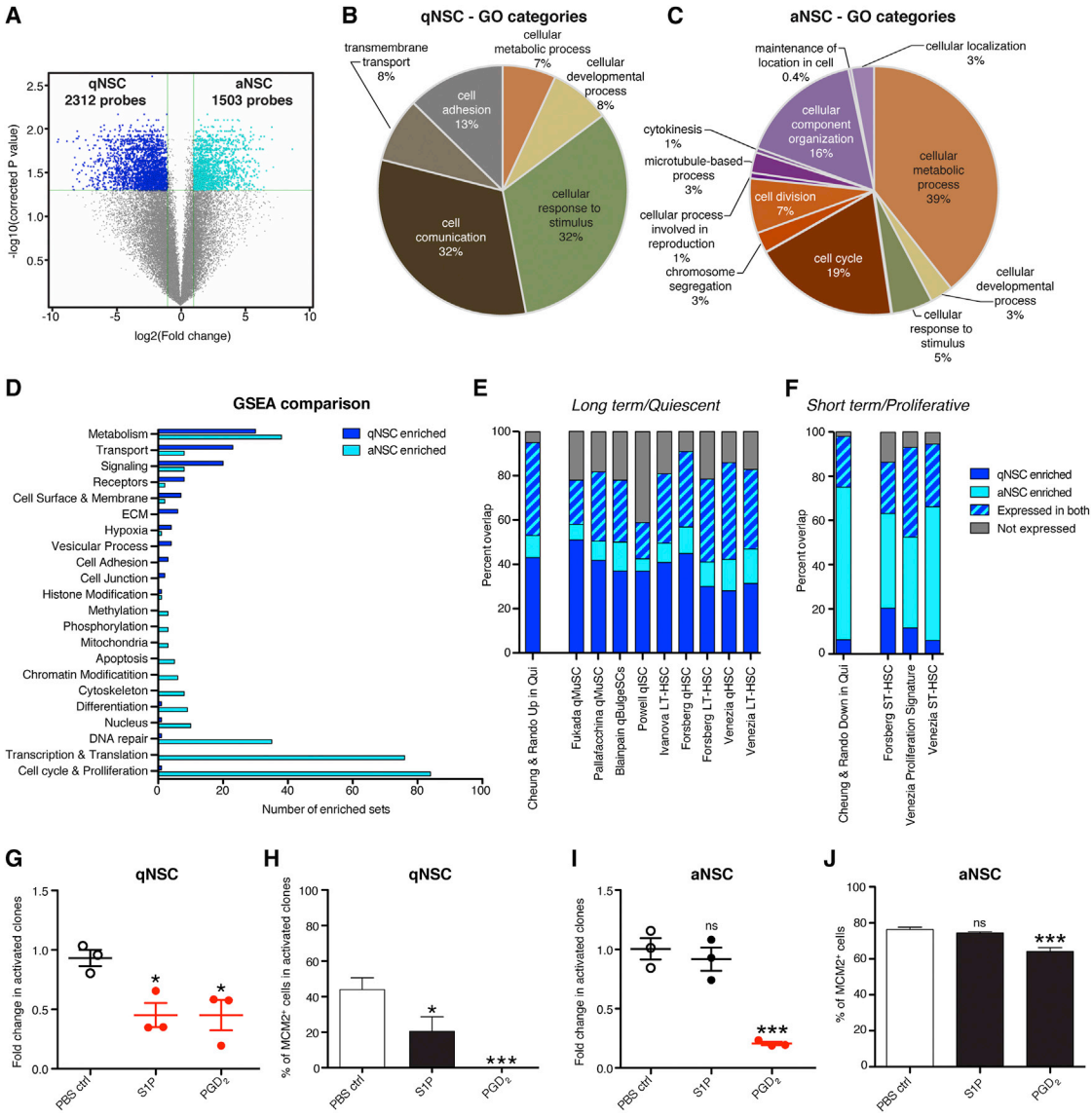

Figure 7. Gene Expression Analysis of qNSCs and aNSCs Reveals Distinct Molecular Signatures

(A) Volcano plot of differentially expressed probesets in qNSCs and aNSCs. Probes have at least 2-fold change in expression and a corrected p value < 0.05.

(B and C) Pie charts showing representative GO categories for differentially expressed probesets in (B) qNSCs and (C) aNSCs, as determined in (A).

(D) GSEA for qNSCs versus aNSCs. Sets have a false discovery rate (q value) <0.05 and are hand curated into thematic categories.

(E and F) Percentage of overlap with signatures of quiescent and dividing stem cells from other organs: (E) long-term (LT)/quiescent signatures and (F) short-term (ST)/proliferative signatures as determined by fold-change analysis of published lists compared to qNSC and aNSC populations. Qui, quiescent; HSC, hematopoietic stem cells; qMuSC, quiescent muscle stem cells; qBulgeSC, quiescent bulge stem cells; qISC, quiescent intestinal stem cells.

(G–J) Targeted GPCR ligand screen. (G) Quantification of qNSC activation (fold change in % Nestin$^+$ clones) as compared to controls (empty dots). (H) Quantification of percentage of MCM2$^+$ cells within activated Nestin$^+$ clones. (I) Quantification of aNSC clones (fold change of percentage of clones that underwent division) as compared to controls (empty dots). (J) Quantification of percentage of MCM2$^+$ aNSCs. Data are represented as means ± SEM.

n = 3. *p < 0.05; ***p < 0.001. ns, not significant.

See also Figure S8 and Tables S1, S2, S3, S4, S5, S6, S7, and S8.

to metabolism of lipids (Figure S8A), which are emerging as important signals in NSC regulation (Knobloch et al., 2013), whereas those in aNSCs were DNA/RNA-related metabolism and proteasome activity (Figure S8B).

Functional studies have implicated numerous genes in the regulation of adult neurogenesis. Many of these were differentially expressed in qNSCs and aNSCs (Table S5). Moreover, direct comparison of qNSC and aNSC transcription profiles with those of purified GFAP::GFP$^+$CD133$^+$ V-SVZ stem cells (Beckervordersandforth et al., 2010) revealed that we have resolved two distinct subsets of NSCs with different molecular and functional properties within their data (Figures S8C and

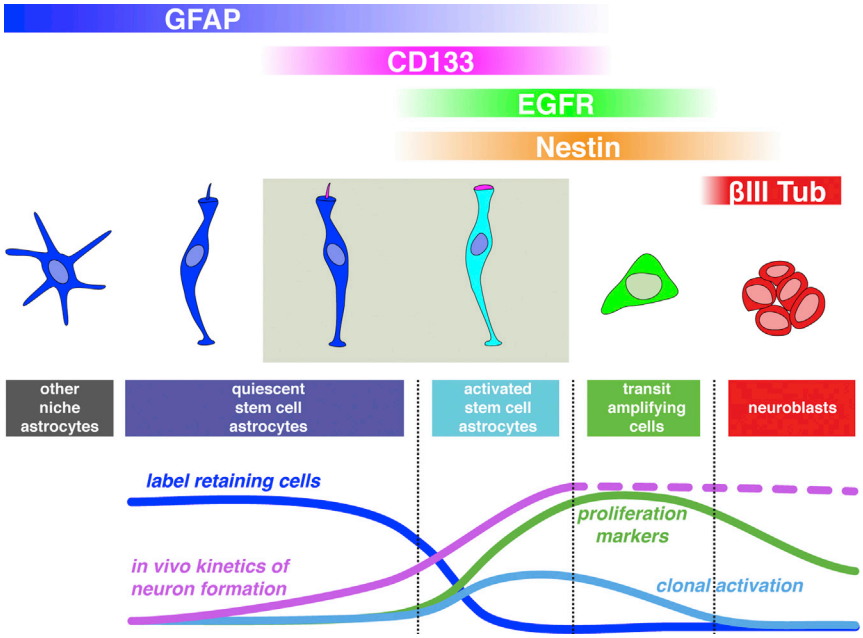

Figure 8. In Vivo and In Vitro Properties of V-SVZ Stem Cells and Their Progeny

Quiescent stem cells ($GFAP^+CD133^+$) are Nestin negative, label-retaining (blue line), and neurogenic in vivo (magenta line) but only very rarely give rise to neurospheres and adherent colonies in vitro (light blue line). Activated stem cells ($GFAP^+CD133^+EGFR^+$) are highly proliferative (green line) and rapidly generate neurons in vivo and are enriched in neurosphere/colony formation. Previous work has shown that $EGFR^+$ transit amplifying cells are also highly proliferative in vivo and give rise to neurospheres. Of note, quiescent stem cells were also present among $CD133^-$ astrocytes. Niche astrocytes have a branched morphology.

S8D; Table S8). Indeed, we found that neurogenic transcription factors such as *Dlx1*, *Dlx2*, *Sox4*, *Sox11*, and *Ascl1*, which were proposed to be hallmarks of NSCs (Beckervordersandforth et al., 2010), were in fact primarily expressed by or restricted to aNSCs (Table S4). We confirmed enrichment of *Dlx2* and *Ascl1* in aNSCs by qRT-PCR (Figures S8F and S8G), as well as enrichment of *Dll1* (Figure S8H), which is expressed in aNSCs (Kawaguchi et al., 2013). In contrast, qNSCs expressed high levels of factors reported to be markers of quiescent stem cells in the adult V-SVZ, such as *Vcam1* (Figure S8I and Table S5; Kokovay et al., 2012), and in other organs, such as *Lrig1* (Figure S8J and Table S1; Jensen and Watt, 2006; Jensen et al., 2009; Powell et al., 2012).

We then performed comparative analysis of our gene expression data with transcriptional signatures from quiescent or proliferative hematopoietic, muscle, skin, and intestinal stem cells (Ivanova et al., 2002; Venezia et al., 2004; Forsberg et al., 2010; Pallafacchina et al., 2010; Powell et al., 2012; Blanpain et al., 2004: Fukada et al., 2007; Cheung and Rando, 2013). The majority of genes in long-term/quiescent populations were upregulated in our quiescent V-SVZ stem cells, whereas those in the short-term/proliferative stem cell lists from other tissues were upregulated in our activated population (Figures 7E and 7F; Table S6). Together, this suggests that common transcriptional programs for quiescence or activation are shared between stem cell lineages in different tissues.

GPCR Signaling Maintains the Quiescent State

To gain insight into signaling pathways that modulate quiescence in qNSCs, we mined our transcriptome data. G protein-coupled receptor (GPCR) signaling was highly enriched in qNSCs (30% of all GSEA signaling sets; Table S3). We selected 25 GPCRs that were more than 10-fold enriched in qNSCs over aNSCs (Table S7) as a basis for a functional screen to assess their role in the regulation of qNSCs. FACS-purified qNSCs were plated under adherent conditions for 4 days in the presence of different ligands, and their activation (number of $Nestin^+$ clones) was quantified (Figure S8K). Two compounds, sphingosine-1-phosphate (S1P) and prostaglandin D_2 (PGD_2), had a significant effect, with both decreasing the activation of qNSCs by approximately one half (Figures 7G and S8L). Both ligands also decreased the number of $MCM2^+$ qNSCs (Figure 7H). PGD_2 exerted a more potent effect, completely abolishing MCM2 expression. To determine whether these compounds act specifically on qNSCs or also affect aNSCs, we plated FACS-purified aNSCs in the presence of S1P or PGD_2 and fixed the cells after 24 hr. This shorter time course is necessary as aNSCs divide very rapidly, making it difficult to distinguish individual clones (Figure S8K). S1P did not alter the number of aNSC clones (Figure 7I) or percentage of $MCM2^+$ cells (Figure 7J). As such, S1P selectively targets qNSCs and appears to act at the level of qNSC recruitment (Figure 7H). In contrast, PGD_2 had a potent inhibitory effect on the number of clones formed by aNSCs (Figure 7I). PGD_2 also reduced the percentage of $MCM2^+$ aNSCs (Figure 7J). As such, PGD_2 acts on both qNSCs and aNSCs. Thus, these GPCR ligands actively maintain the adult NSC quiescent state.

DISCUSSION

Here, we prospectively identified and isolated quiescent adult NSCs by defining a combination of markers (CD133, GFAP, and EGFR) that allows the simultaneous purification of quiescent and activated populations of stem cell astrocytes. Together, our analyses of their cell cycle properties, their morphological and anatomical localization, their in vitro and in vivo functional behavior, and their gene expression profiles highlight the distinct functional and molecular properties of qNSCs and aNSCs (Figure 8). Our functional analyses reveal important features of quiescent NSCs, which affect the interpretation of commonly used in vitro NSC assays and lineage-tracing strategies.

In the adult mouse brain, CD133 was originally proposed to be exclusively expressed by ependymal cells, with FACS-purified $CD133^+$ cells giving rise to neurospheres in vitro and generating neurons in vivo (Coskun et al., 2008). However, CD133 is also expressed by a subset of astrocytes, which behave as NSCs (Mirzadeh et al., 2008; Beckervordersandforth et al., 2010), suggesting that the earlier findings can be attributed to $CD133^+$ astrocytes instead of ependymal cells. Here, we show that CD133 is expressed by both quiescent and activated V-SVZ stem cells.

The neurosphere assay is widely used as a readout of in vivo stem cells (reviewed in Pastrana et al., 2011). Neurospheres were originally proposed to arise from relatively quiescent stem cells in vivo (Morshead et al., 1994). With the ability to prospectively purify cells at different stages of the stem cell lineage, it is now feasible to directly assess the potential of distinct populations to give rise to neurospheres. Here, we show that qNSCs only very rarely give rise to either neurospheres or adherent colonies and do not increase their neurosphere-forming efficiency during regeneration. In contrast, aNSCs are enriched in neurosphere and adherent colony formation. Together, our current findings and previous reports highlight that the major source of neurosphere-initiating cells are actively dividing in vivo, and include both $GFAP^+$ aNSCs and $EGFR^+GFAP^-$ transit-amplifying cells (Doetsch et al., 2002, Imura et al., 2003; Morshead et al., 2003; Garcia et al., 2004, Pastrana et al., 2009; data not shown). Thus, the neurosphere assay is a useful tool for assessing the in vitro stem cell potential of proliferative populations but does not allow the identification and enumeration of in vivo quiescent stem cells. This emphasizes the need to develop novel assays, or identify additional niche factors, that allow qNSCs to be expanded in vitro.

Nestin is frequently used both as a marker of NSCs and for their genetic manipulation and lineage tracing in the embryonic (Lendahl et al., 1990; Zimmerman et al., 1994) and adult brain (reviewed in Imayoshi et al., 2011). $Nestin^+$ cells have also been implicated as putative glioblastoma-forming cells (Holland et al., 2000, Chen et al., 2012). Notably, we found that adult V-SVZ qNSCs do not express Nestin but upregulate it on activation in vitro, as well as during regeneration in vivo. These data are consistent with previous observations that $Nestin^-/CD133^+$ cells are neurogenic in vivo and give rise to $Nestin^+$ neurospheres in vitro (Coskun et al., 2008). Recently, both Nestin-negative and Nestin-positive radial glia-like stem cells have also been described in the hippocampus (DeCarolis et al., 2013). As we show here in the V-SVZ, in the SGZ, almost all of the dividing radial glia-like stem cells express Nestin (DeCarolis et al., 2013). It is interesting that, in embryonic development, Nestin expression is also regulated in a cell-cycle-dependent manner (Sunabori et al., 2008). Thus, Nestin expression is dynamically regulated in NSCs. Importantly, our study highlights that Nestin immunostaining cannot be used to identify adult qNSCs in vivo. Thus, whether recombination and reporter expression occur in qNSCs needs to be carefully assessed when using Nestin transgenes for in vivo targeting of adult NSCs, V-SVZ lineage tracing, genetic manipulation, or purification. Moreover, interpretation of such assays is further complicated by the high expression of Nestin in ependymal cells, which can lead to nonautonomous effects.

qNSCs are multipotent and self-renewing in vitro. In vivo, qNSCs are long-term neurogenic and exhibit delayed kinetics of neuron formation compared to aNSCs. Interestingly, some aNSC transplants also continue to make neurons 30 days after transplantation. These may arise from a more quiescent subpopulation of aNSCs or from aNSCs that have reverted back to the quiescent state, as occurs in vitro. We also observed oligodendrocyte formation by both transplanted qNSCs and aNSCs (data not shown). In vivo, adult V-SVZ NSCs have regional identity and generate distinct neuronal subtypes, or oligodendrocytes (Merkle et al., 2007; Ventura and Goldman, 2007; Young et al., 2007; Ortega et al., 2013). At present, we cannot distinguish whether neurons and oligodendrocytes arise from regionally distinct subpopulations of NSCs in the transplanted populations or whether some, or all, NSCs are multipotent in vivo. The extent of in vivo V-SVZ stem cell heterogeneity and population dynamics of qNSCs and aNSCs, as well as their lineage relationships and potential under homeostasis and during regeneration, will require the identification of novel markers allowing the specific targeting of qNSCs and aNSCs. Importantly, our present strategy allows qNSCs to be isolated irrespective of their regional origin. Of note, the $GFAP::GFP^+$ $CD133^-$ population also contains quiescent stem cells. By combining different reporter mice, it is emerging that V-SVZ stem cells are molecularly heterogeneous (Giachino et al., 2014). The iterative identification of additional markers that allow subpopulations of NSCs to be isolated and targeted in vivo is a key future step.

Recent findings suggest that quiescent and activated states are differentially regulated at multiple levels, including cell-cell and extracellular matrix interactions, diffusible signals and distinct transcriptional programs coupling cell cycle regulators, quiescence, self-renewal, and differentiation (Kazanis et al., 2010; Young et al., 2011; Le Belle et al., 2011; Alfonso et al., 2012; Basak et al., 2012; Marqués-Torrejón et al., 2013; Kokovay et al., 2012; Porlan et al., 2013; Giachino et al., 2014; Kawaguchi et al., 2013, López-Juárez et al., 2013; Martynoga et al., 2013). Our transcriptome data of qNSCs and aNSCs isolated directly from their in vivo niche provide a platform to functionally assess the gene regulatory networks active in each state. Interestingly, our GSEA analysis reveals that GPCR signaling is specifically enriched in qNSCs. While GPCRs modulate many different facets of adult neurogenesis (Doze and Perez, 2012), our findings highlight that they are also key regulators of qNSCs. Strikingly, both functional ligands we identify in our GPCR screen, S1P and PGD_2, inhibit the activation of qNSCs, suggesting that stem cell quiescence is an actively maintained state. Both S1P and PGD_2 are present in the CSF (Sato et al., 2007; Kondabolu et al., 2011), which is emerging as a reservoir of factors in the embryo and the adult important for stem cell regulation (Silva-Vargas et al., 2013). As such, the CSF may be a key niche compartment mediating quiescence in the adult V-SVZ. Interestingly, PGD_2 has been implicated in promoting the quiescent phase of the hair follicle cycle (Garza et al., 2012), which is consistent with our transcriptome data suggesting that quiescent and activated stem cells in different tissues share common molecular pathways.

As additional mediators of stem cell quiescence and activation are uncovered, it will be important to investigate how clinical drugs targeting these pathways impact NSCs in vivo. For instance, fingolimod, an immunomodulatory drug approved by the Food and Drug Administration for the treatment of multiple sclerosis (Kappos et al., 2006), acts on S1P receptors. Recent studies have shown that fingolimod also acts on multiple CNS cell types (Groves et al., 2013), including astrocytes. Our identification of S1P as a regulator of stem cell quiescence suggests that this drug may have an effect on NSCs in the adult brain.

The ability to purify quiescent NSCs from the adult brain opens new vistas into elucidating the biology of stem cell quiescence, enabling studies in their intrinsic and extrinsic molecular regulation and defining their dynamics during development and aging. V-SVZ GFAP$^+$ stem cells are also present in humans, where they are largely quiescent (Sanai et al., 2004, 2011; van den Berge et al., 2010). Understanding the biology of stem cell quiescence and activation will ultimately lead to insight into how NSCs contribute to brain pathology and can be harnessed for brain repair.

EXPERIMENTAL PROCEDURES

Animal Use

Experiments were performed in accordance with Columbia University institutional and national guidelines for animal use. All mice used were between 2 and 3 months old.

FACS

The FACS strategy was adapted from Pastrana et al. (2009). Briefly, the V-SVZ was microdissected from GFAP::GFP mice and dissociated with papain, the single cell suspension was immunostained, and cell populations were purified by FACS as described in the detailed protocol in Supplemental Experimental Procedures.

Immunostaining

Whole mounts were dissected and processed as described elsewhere (Doetsch et al., 1999b; Tavazoie et al., 2008; Mirzadeh et al., 2010). Briefly, whole mounts were blocked in 10% serum, incubated with primary antibodies for 48 hr at 4°C, revealed with secondary antibodies, and imaged with a Zeiss LSM510 or Leica TCS SP5 II confocal microscope. All immunostainings were performed in triplicate. Immunostaining details for whole mounts and cell cultures are in the Supplemental Experimental Procedures.

In Vitro Assays

For neurosphere assays, FACS-purified cells were collected in neurosphere medium without growth factors and plated at clonal density with EGF (20 ng/ml) or EGF/bFGF (20 ng/ml each). For adherent cultures, purified cells were collected in neurosphere medium and plated on poly-D-lysine and fibronectin-coated 96-well plates as single cells or at clonal density and cultured with EGF or EGF/bFGF. Further details are given in the Supplemental Experimental Procedures.

Ara-C Infusion

A micro-osmotic pump (ALZET, 1007D) filled with 2% Ara-C (Sigma) in 0.9% saline was implanted on to the surface of the brain as described elsewhere (Doetsch et al., 1999b). After 6 days of Ara-C infusion, mice were sacrificed either immediately or 12 hr after pump removal.

Electroporation

One microliter of a solution containing 5 μg/μl of the mP2-mCherry plasmid in 0.9% saline was electroporated according to Barnabé-Heider et al. (2008), using the following coordinates: anterior-posterior (AP), 0.0; lateral (L), 0.85; ventral (V), −2.5 mm relative to bregma. The mP2-mCherry plasmid was made by cloning the mouse P2 element of the Prominin1 promoter into the CherryPicker control vector (Clontech), using the *XhoI* and *AgeI* digestion sites. See the Supplemental Information for details.

Transplants

Three injections of 0.2 μl delivering 1,000–3,000 cells purified from GFAP::GFP/β-actin-PLAP mice were performed in the SVZ of wild-type recipient mice, using the following coordinates: (1) AP, 0.0; L, 1.4; V, −2.1; (2) AP, 0.5; L, 1.1; V, −2.2; (3) AP, 1.0; L, 1.0; V, −2.5 mm relative to bregma. Recipient mice were sacrificed 1 week or 1 month after transplantation. Transplanted cells were revealed by NBT/BCIP staining.

RNA Isolation and Microarray Hybridization

RNA was purified from FACS-sorted populations with the miRNeasy kit (QIAGEN) from three biological replicates. cDNA was synthesized with the Nugen Pico amplification kit and hybridized to Affymetrix MOE430.2 chips. See Supplemental Information for details of the bioinformatic analysis.

qRT-PCR

RNA was purified from FACS-sorted populations with the miRNeasy kit (QIAGEN) and cDNA generated using WT-Ovation Pico System (NuGEN). See Supplemental Information for details on primer sequences.

GPCR Compound Screen

Cells were isolated by FACS and plated on poly-D-lysine- and fibronectin-coated 96-well plates in the presence of EGF. To assay the effect on qNSCs, compounds were added 1 day after plating, and cells were fixed and immunostained at day 4. To assay the effect on aNSCs, cells were plated with compounds and fixed and immunostained 1 day later. Further details are in the Supplemental Experimental Procedures.

ACCESSION NUMBERS

All data are deposited in the National Center for Biotechnology Information Gene Expression Omnibus under accession number GSE54653.

SUPPLEMENTAL INFORMATION

Supplemental Information includes Supplemental Experimental Procedures, eight figures, and eight tables and can be found with this article online at http://dx.doi.org/10.1016/j.neuron.2014.02.039.

ACKNOWLEDGMENTS

Thanks to the F.D. and Wichterle labs for insightful discussion and to Hynek Wichterle and Jun-An Chen for comments. We thank Hideyuki Okano for kindly providing the Nestin::Kusabira Orange and James Stringer for providing the alkaline phosphatase reporter mice; Kristie Gordon and Sandra Tetteh of the Herbert Irving Comprehensive Cancer Center of Columbia University for assistance with FACS and flow cytometry; and Jiri Zavadil and Yutong Zhang of the Office of Collaborative Science Genome Technology Center of New York University Langone Medical Center for microarray processing. This work was supported by the National Institute of Neurological Disorders and Stroke (NINDS) grant NS053884, funding from the NINDS-American Recovery and Reinvestment Act (NS053884-03S109), NINDS grant NS074039, New York State Stem Cell Science contracts C024287 and C026401, funding from The Leona M. and Harry B. Helmsley Charitable Trust, The Irma T. Hirschl Foundation, and The David and Lucile Packard Foundation (to F.D.); a Human Frontiers Scientific Program Long-Term Fellowship (to V.S-V.); NIH grant T32 MH 15174-29 and a fellowship from the Spanish Ministerio de Educación y Ciencia (to E.P.); NINDS grant 1F31NS079057 (to A.R.M.-S.), and NIH grants T32 GM008224, TL1 TR000082 and NINDS grant 1F31NS081990 (to A.M.D.). Work was also supported by the Jerry and Emily Spiegel Laboratory for Cell Replacement Therapies.

Accepted: February 10, 2014
Published: May 7, 2014

REFERENCES

Ahn, S., and Joyner, A.L. (2005). In vivo analysis of quiescent adult neural stem cells responding to Sonic hedgehog. Nature *437*, 894–897.

Alfonso, J., Le Magueresse, C., Zuccotti, A., Khodosevich, K., and Monyer, H. (2012). Diazepam binding inhibitor promotes progenitor proliferation in the postnatal SVZ by reducing GABA signaling. Cell Stem Cell *10*, 76–87.

Barnabé-Heider, F., Meletis, K., Eriksson, M., Bergmann, O., Sabelström, H., Harvey, M.A., Mikkers, H., and Frisén, J. (2008). Genetic manipulation of adult mouse neurogenic niches by in vivo electroporation. Nat. Methods *5*, 189–196.

Basak, O., Giachino, C., Fiorini, E., Macdonald, H.R., and Taylor, V. (2012). Neurogenic subventricular zone stem/progenitor cells are Notch1-dependent in their active but not quiescent state. J. Neurosci. *32*, 5654–5666.

Beckervordersandforth, R., Tripathi, P., Ninkovic, J., Bayam, E., Lepier, A., Stempfhuber, B., Kirchhoff, F., Hirrlinger, J., Haslinger, A., Lie, D.C., et al. (2010). In vivo fate mapping and expression analysis reveals molecular hallmarks of prospectively isolated adult neural stem cells. Cell Stem Cell *7*, 744–758.

Blanpain, C., Lowry, W.E., Geoghegan, A., Polak, L., and Fuchs, E. (2004). Self-renewal, multipotency, and the existence of two cell populations within an epithelial stem cell niche. Cell *118*, 635–648.

Cesetti, T., Fila, T., Obernier, K., Bengtson, C.P., Li, Y., Mandl, C., Hölzl-Wenig, G., and Ciccolini, F. (2011). GABAA receptor signaling induces osmotic swelling and cell cycle activation of neonatal prominin+ precursors. Stem Cells *29*, 307–319.

Chen, J., Li, Y., Yu, T.S., McKay, R.M., Burns, D.K., Kernie, S.G., and Parada, L.F. (2012). A restricted cell population propagates glioblastoma growth after chemotherapy. Nature *488*, 522–526.

Cheung, T.H., and Rando, T.A. (2013). Molecular regulation of stem cell quiescence. Nat. Rev. Mol. Cell Biol. *14*, 329–340.

Coskun, V., Wu, H., Blanchi, B., Tsao, S., Kim, K., Zhao, J., Biancotti, J.C., Hutnick, L., Krueger, R.C., Jr., Fan, G., et al. (2008). CD133+ neural stem cells in the ependyma of mammalian postnatal forebrain. Proc. Natl. Acad. Sci. USA *105*, 1026–1031.

DeCarolis, N.A., Mechanic, M., Petrik, D., Carlton, A., Ables, J.L., Malhotra, S., Bachoo, R., Götz, M., Lagace, D.C., and Eisch, A.J. (2013). In vivo contribution of nestin- and GLAST-lineage cells to adult hippocampal neurogenesis. Hippocampus *23*, 708–719.

DePrimo, S.E., Stambrook, P.J., and Stringer, J.R. (1996). Human placental alkaline phosphatase as a histochemical marker of gene expression in transgenic mice. Transgenic Res. *5*, 459–466.

Doetsch, F., García-Verdugo, J.M., and Alvarez-Buylla, A. (1997). Cellular composition and three-dimensional organization of the subventricular germinal zone in the adult mammalian brain. J. Neurosci. *17*, 5046–5061.

Doetsch, F., Caillé, I., Lim, D.A., García-Verdugo, J.M., and Alvarez-Buylla, A. (1999a). Subventricular zone astrocytes are neural stem cells in the adult mammalian brain. Cell *97*, 703–716.

Doetsch, F., García-Verdugo, J.M., and Alvarez-Buylla, A. (1999b). Regeneration of a germinal layer in the adult mammalian brain. Proc. Natl. Acad. Sci. USA *96*, 11619–11624.

Doetsch, F., Petreanu, L., Caillé, I., Garcia-Verdugo, J.M., and Alvarez-Buylla, A. (2002). EGF converts transit-amplifying neurogenic precursors in the adult brain into multipotent stem cells. Neuron *36*, 1021–1034.

Doze, V.A., and Perez, D.M. (2012). G-protein-coupled receptors in adult neurogenesis. Pharmacol. Rev. *64*, 645–675.

Forsberg, E.C., Passegué, E., Prohaska, S.S., Wagers, A.J., Koeva, M., Stuart, J.M., and Weissman, I.L. (2010). Molecular signatures of quiescent, mobilized and leukemia-initiating hematopoietic stem cells. PLoS ONE *5*, e8785.

Fukada, S., Uezumi, A., Ikemoto, M., Masuda, S., Segawa, M., Tanimura, N., Yamamoto, H., Miyagoe-Suzuki, Y., and Takeda, S. (2007). Molecular signature of quiescent satellite cells in adult skeletal muscle. Stem Cells *25*, 2448–2459.

Garcia, A.D.R., Doan, N.B., Imura, T., Bush, T.G., and Sofroniew, M.V. (2004). GFAP-expressing progenitors are the principal source of constitutive neurogenesis in adult mouse forebrain. Nat. Neurosci. *7*, 1233–1241.

Garza, L.A., Liu, Y., Yang, Z., Alagesan, B., Lawson, J.A., Norberg, S.M., Loy, D.E., Zhao, T., Blatt, H.B., Stanton, D.C., et al. (2012). Prostaglandin D2 inhibits hair growth and is elevated in bald scalp of men with androgenetic alopecia. Sci. Transl. Med. *4*, 126ra34.

Giachino, C., and Taylor, V. (2009). Lineage analysis of quiescent regenerative stem cells in the adult brain by genetic labelling reveals spatially restricted neurogenic niches in the olfactory bulb. Eur. J. Neurosci. *30*, 9–24.

Giachino, C., Basak, O., Lugert, S., Knuckles, P., Obernier, K., Fiorelli, R., Frank, S., Raineteau, O., Alvarez-Buylla, A., and Taylor, V. (2014). Molecular diversity subdivides the adult forebrain neural stem cell population. Stem Cells *32*, 70–84.

Graham, V., Khudyakov, J., Ellis, P., and Pevny, L. (2003). SOX2 functions to maintain neural progenitor identity. Neuron *39*, 749–765.

Groves, A., Kihara, Y., and Chun, J. (2013). Fingolimod: direct CNS effects of sphingosine 1-phosphate (S1P) receptor modulation and implications in multiple sclerosis therapy. J. Neurol. Sci. *328*, 9–18.

Holland, E.C., Celestino, J., Dai, C., Schaefer, L., Sawaya, R.E., and Fuller, G.N. (2000). Combined activation of Ras and Akt in neural progenitors induces glioblastoma formation in mice. Nat. Genet. *25*, 55–57.

Imayoshi, I., Sakamoto, M., and Kageyama, R. (2011). Genetic methods to identify and manipulate newly born neurons in the adult brain. Front. Neurosci. *5*, 64.

Imura, T., Kornblum, H.I., and Sofroniew, M.V. (2003). The predominant neural stem cell isolated from postnatal and adult forebrain but not early embryonic forebrain expresses GFAP. J. Neurosci. *23*, 2824–2832.

Ishizuka, K., Kamiya, A., Oh, E.C., Kanki, H., Seshadri, S., Robinson, J.F., Murdoch, H., Dunlop, A.J., Kubo, K., Furukori, K., et al. (2011). DISC1-dependent switch from progenitor proliferation to migration in the developing cortex. Nature *473*, 92–96.

Ivanova, N.B., Dimos, J.T., Schaniel, C., Hackney, J.A., Moore, K.A., and Lemischka, I.R. (2002). A stem cell molecular signature. Science *298*, 601–604.

Jensen, K.B., and Watt, F.M. (2006). Single-cell expression profiling of human epidermal stem and transit-amplifying cells: Lrig1 is a regulator of stem cell quiescence. Proc. Natl. Acad. Sci. USA *103*, 11958–11963.

Jensen, K.B., Collins, C.A., Nascimento, E., Tan, D.W., Frye, M., Itami, S., and Watt, F.M. (2009). Lrig1 expression defines a distinct multipotent stem cell population in mammalian epidermis. Cell Stem Cell *4*, 427–439.

Kanki, H., Shimabukuro, M.K., Miyawaki, A., and Okano, H. (2010). "Color Timer" mice: visualization of neuronal differentiation with fluorescent proteins. Mol. Brain *3*, 5.

Kappos, L., Antel, J., Comi, G., Montalban, X., O'Connor, P., Polman, C.H., Haas, T., Korn, A.A., Karlsson, G., and Radue, E.W.; FTY720 D2201 Study Group (2006). Oral fingolimod (FTY720) for relapsing multiple sclerosis. N. Engl. J. Med. *355*, 1124–1140.

Kawaguchi, D., Furutachi, S., Kawai, H., Hozumi, K., and Gotoh, Y. (2013). Dll1 maintains quiescence of adult neural stem cells and segregates asymmetrically during mitosis. Nat Commun *4*, 1880.

Kazanis, I., Lathia, J.D., Vadakkan, T.J., Raborn, E., Wan, R., Mughal, M.R., Eckley, D.M., Sasaki, T., Patton, B., Mattson, M.P., et al. (2010). Quiescence and activation of stem and precursor cell populations in the subependymal zone of the mammalian brain are associated with distinct cellular and extracellular matrix signals. J. Neurosci. *30*, 9771–9781.

Knobloch, M., Braun, S.M., Zurkirchen, L., von Schoultz, C., Zamboni, N., Araúzo-Bravo, M.J., Kovacs, W.J., Karalay, O., Suter, U., Machado, R.A., et al. (2013). Metabolic control of adult neural stem cell activity by Fasn-dependent lipogenesis. Nature *493*, 226–230.

Kokovay, E., Goderie, S., Wang, Y., Lotz, S., Lin, G., Sun, Y., Roysam, B., Shen, Q., and Temple, S. (2010). Adult SVZ lineage cells home to and leave

the vascular niche via differential responses to SDF1/CXCR4 signaling. Cell Stem Cell *7*, 163–173.

Kokovay, E., Wang, Y., Kusek, G., Wurster, R., Lederman, P., Lowry, N., Shen, Q., and Temple, S. (2012). VCAM1 is essential to maintain the structure of the SVZ niche and acts as an environmental sensor to regulate SVZ lineage progression. Cell Stem Cell *11*, 220–230.

Kondabolu, S., Adsumelli, R., Schabel, J., Glass, P., and Pentyala, S. (2011). Evaluation of prostaglandin D2 as a CSF leak marker: implications in safe epidural anesthesia. Local Reg. Anesth. *4*, 21–24.

Lacar, B., Young, S.Z., Platel, J.C., and Bordey, A. (2011). Gap junction-mediated calcium waves define communication networks among murine postnatal neural progenitor cells. Eur. J. Neurosci. *34*, 1895–1905.

Lacar, B., Herman, P., Platel, J.C., Kubera, C., Hyder, F., and Bordey, A. (2012). Neural progenitor cells regulate capillary blood flow in the postnatal subventricular zone. J. Neurosci. *32*, 16435–16448.

Laywell, E.D., Rakic, P., Kukekov, V.G., Holland, E.C., and Steindler, D.A. (2000). Identification of a multipotent astrocytic stem cell in the immature and adult mouse brain. Proc. Natl. Acad. Sci. USA *97*, 13883–13888.

Le Belle, J.E., Orozco, N.M., Paucar, A.A., Saxe, J.P., Mottahedeh, J., Pyle, A.D., Wu, H., and Kornblum, H.I. (2011). Proliferative neural stem cells have high endogenous ROS levels that regulate self-renewal and neurogenesis in a PI3K/Akt-dependant manner. Cell Stem Cell *8*, 59–71.

Lee, C., Hu, J., Ralls, S., Kitamura, T., Loh, Y.P., Yang, Y., Mukouyama, Y.S., and Ahn, S. (2012). The molecular profiles of neural stem cell niche in the adult subventricular zone. PLoS ONE *7*, e50501.

Lendahl, U., Zimmerman, L.B., and McKay, R.D. (1990). CNS stem cells express a new class of intermediate filament protein. Cell *60*, 585–595.

Li, L., and Clevers, H. (2010). Coexistence of quiescent and active adult stem cells in mammals. Science *327*, 542–545.

López-Juárez, A., Howard, J., Ullom, K., Howard, L., Grande, A., Pardo, A., Waclaw, R., Sun, Y.Y., Yang, D., Kuan, C.Y., et al. (2013). Gsx2 controls region-specific activation of neural stem cells and injury-induced neurogenesis in the adult subventricular zone. Genes Dev. *27*, 1272–1287.

Marqués-Torrejón, M.Á., Porlan, E., Banito, A., Gómez-Ibarlucea, E., Lopez-Contreras, A.J., Fernández-Capetillo, O., Vidal, A., Gil, J., Torres, J., and Fariñas, I. (2013). Cyclin-dependent kinase inhibitor p21 controls adult neural stem cell expansion by regulating Sox2 gene expression. Cell Stem Cell *12*, 88–100.

Martynoga, B., Mateo, J.L., Zhou, B., Andersen, J., Achimastou, A., Urbán, N., van den Berg, D., Georgopoulou, D., Hadjur, S., Wittbrodt, J., et al. (2013). Epigenomic enhancer annotation reveals a key role for NFIX in neural stem cell quiescence. Genes Dev. *27*, 1769–1786.

Marzesco, A.-M., Janich, P., Wilsch-Bräuninger, M., Dubreuil, V., Langenfeld, K., Corbeil, D., and Huttner, W.B. (2005). Release of extracellular membrane particles carrying the stem cell marker prominin-1 (CD133) from neural progenitors and other epithelial cells. J. Cell Sci. *118*, 2849–2858.

Maslov, A.Y., Barone, T.A., Plunkett, R.J., and Pruitt, S.C. (2004). Neural stem cell detection, characterization, and age-related changes in the subventricular zone of mice. J. Neurosci. *24*, 1726–1733.

Merkle, F.T., Mirzadeh, Z., and Alvarez-Buylla, A. (2007). Mosaic organization of neural stem cells in the adult brain. Science *317*, 381–384.

Mirzadeh, Z., Merkle, F.T., Soriano-Navarro, M., Garcia-Verdugo, J.M., and Alvarez-Buylla, A. (2008). Neural stem cells confer unique pinwheel architecture to the ventricular surface in neurogenic regions of the adult brain. Cell Stem Cell *3*, 265–278.

Mirzadeh, Z., Doetsch, F., Sawamoto, K., Wichterle, H., and Alvarez-Buylla, A. (2010). The subventricular zone en-face: wholemount staining and ependymal flow. J. Vis. Exp. (39) http://dx.doi.org/10.3791/1938.

Morshead, C.M., Reynolds, B.A., Craig, C.G., McBurney, M.W., Staines, W.A., Morassutti, D., Weiss, S., and van der Kooy, D. (1994). Neural stem cells in the adult mammalian forebrain: a relatively quiescent subpopulation of subependymal cells. Neuron *13*, 1071–1082.

Morshead, C.M., Garcia, A.D., Sofroniew, M.V., and van Der Kooy, D. (2003). The ablation of glial fibrillary acidic protein-positive cells from the adult central nervous system results in the loss of forebrain neural stem cells but not retinal stem cells. Eur. J. Neurosci. *18*, 76–84.

Nam, H.-S., and Benezra, R. (2009). High levels of Id1 expression define B1 type adult neural stem cells. Cell Stem Cell *5*, 515–526.

Ortega, F., Gascón, S., Masserdotti, G., Deshpande, A., Simon, C., Fischer, J., Dimou, L., Chichung Lie, D., Schroeder, T., and Berninger, B. (2013). Oligodendrogliogenic and neurogenic adult subependymal zone neural stem cells constitute distinct lineages and exhibit differential responsiveness to Wnt signalling. Nat. Cell Biol. *15*, 602–613.

Pallafacchina, G., François, S., Regnault, B., Czarny, B., Dive, V., Cumano, A., Montarras, D., and Buckingham, M. (2010). An adult tissue-specific stem cell in its niche: a gene profiling analysis of in vivo quiescent and activated muscle satellite cells. Stem Cell Res. (Amst.) *4*, 77–91.

Pastrana, E., Cheng, L.-C., and Doetsch, F. (2009). Simultaneous prospective purification of adult subventricular zone neural stem cells and their progeny. Proc. Natl. Acad. Sci. USA *106*, 6387–6392.

Pastrana, E., Silva-Vargas, V., and Doetsch, F. (2011). Eyes wide open: a critical review of sphere-formation as an assay for stem cells. Cell Stem Cell *8*, 486–498.

Pinto, L., Mader, M.T., Irmler, M., Gentilini, M., Santoni, F., Drechsel, D., Blum, R., Stahl, R., Bulfone, A., Malatesta, P., et al. (2008). Prospective isolation of functionally distinct radial glial subtypes—lineage and transcriptome analysis. Mol. Cell. Neurosci. *38*, 15–42.

Platel, J.C., Gordon, V., Heintz, T., and Bordey, A. (2009). GFAP-GFP neural progenitors are antigenically homogeneous and anchored in their enclosed mosaic niche. Glia *57*, 66–78.

Ponti, G., Obernier, K., Guinto, C., Jose, L., Bonfanti, L., and Alvarez-Buylla, A. (2013). Cell cycle and lineage progression of neural progenitors in the ventricular-subventricular zones of adult mice. Proc. Natl. Acad. Sci. USA *110*, E1045–E1054.

Porlan, E., Morante-Redolat, J.M., Marqués-Torrejón, M.Á., Andreu-Agulló, C., Carneiro, C., Gómez-Ibarlucea, E., Soto, A., Vidal, A., Ferrón, S.R., and Fariñas, I. (2013). Transcriptional repression of Bmp2 by p21(Waf1/Cip1) links quiescence to neural stem cell maintenance. Nat. Neurosci. *16*, 1567–1575.

Powell, A.E., Wang, Y., Li, Y., Poulin, E.J., Means, A.L., Washington, M.K., Higginbotham, J.N., Juchheim, A., Prasad, N., Levy, S.E., et al. (2012). The pan-ErbB negative regulator Lrig1 is an intestinal stem cell marker that functions as a tumor suppressor. Cell *149*, 146–158.

Sanai, N., Tramontin, A.D., Quiñones-Hinojosa, A., Barbaro, N.M., Gupta, N., Kunwar, S., Lawton, M.T., McDermott, M.W., Parsa, A.T., Manuel-García Verdugo, J., et al. (2004). Unique astrocyte ribbon in adult human brain contains neural stem cells but lacks chain migration. Nature *427*, 740–744.

Sanai, N., Nguyen, T., Ihrie, R.A., Mirzadeh, Z., Tsai, H.H., Wong, M., Gupta, N., Berger, M.S., Huang, E., Garcia-Verdugo, J.M., et al. (2011). Corridors of migrating neurons in the human brain and their decline during infancy. Nature *478*, 382–386.

Sato, K., Malchinkhuu, E., Horiuchi, Y., Mogi, C., Tomura, H., Tosaka, M., Yoshimoto, Y., Kuwabara, A., and Okajima, F. (2007). HDL-like lipoproteins in cerebrospinal fluid affect neural cell activity through lipoprotein-associated sphingosine 1-phosphate. Biochem. Biophys. Res. Commun. *359*, 649–654.

Shen, Q., Wang, Y., Kokovay, E., Lin, G., Chuang, S.-M., Goderie, S.K., Roysam, B., and Temple, S. (2008). Adult SVZ stem cells lie in a vascular niche: a quantitative analysis of niche cell-cell interactions. Cell Stem Cell *3*, 289–300.

Silva-Vargas, V., Crouch, E.E., and Doetsch, F. (2013). Adult neural stem cells and their niche: a dynamic duo during homeostasis, regeneration, and aging. Curr. Opin. Neurobiol. *23*, 935–942.

Subramanian, A., Tamayo, P., Mootha, V.K., Mukherjee, S., Ebert, B.L., Gillette, M.A., Paulovich, A., Pomeroy, S.L., Golub, T.R., Lander, E.S., and Mesirov, J.P. (2005). Gene set enrichment analysis: a knowledge-based approach for interpreting genome-wide expression profiles. Proc. Natl. Acad. Sci. USA *102*, 15545–15550.

Sun, Y., Kong, W., Falk, A., Hu, J., Zhou, L., Pollard, S., and Smith, A. (2009). CD133 (Prominin) negative human neural stem cells are clonogenic and tripotent. PLoS ONE *4*, e5498.

Sunabori, T., Tokunaga, A., Nagai, T., Sawamoto, K., Okabe, M., Miyawaki, A., Matsuzaki, Y., Miyata, T., and Okano, H. (2008). Cell-cycle-specific nestin expression coordinates with morphological changes in embryonic cortical neural progenitors. J. Cell Sci. *121*, 1204–1212.

Tavazoie, M., Van der Veken, L., Silva-Vargas, V., Louissaint, M., Colonna, L., Zaidi, B., Garcia-Verdugo, J.M., and Doetsch, F. (2008). A specialized vascular niche for adult neural stem cells. Cell Stem Cell *3*, 279–288.

Uchida, N., Buck, D.W., He, D., Reitsma, M.J., Masek, M., Phan, T.V., Tsukamoto, A.S., Gage, F.H., and Weissman, I.L. (2000). Direct isolation of human central nervous system stem cells. Proc. Natl. Acad. Sci. USA *97*, 14720–14725.

van den Berge, S.A., Middeldorp, J., Zhang, C.E., Curtis, M.A., Leonard, B.W., Mastroeni, D., Voorn, P., van de Berg, W.D., Huitinga, I., and Hol, E.M. (2010). Longterm quiescent cells in the aged human subventricular neurogenic system specifically express GFAP-delta. Aging Cell *9*, 313–326.

Venezia, T.A., Merchant, A.A., Ramos, C.A., Whitehouse, N.L., Young, A.S., Shaw, C.A., and Goodell, M.A. (2004). Molecular signatures of proliferation and quiescence in hematopoietic stem cells. PLoS Biol. *2*, e301.

Ventura, R.E., and Goldman, J.E. (2007). Dorsal radial glia generate olfactory bulb interneurons in the postnatal murine brain. J. Neurosci. *27*, 4297–4302.

Wilson, A., Laurenti, E., Oser, G., van der Wath, R.C., Blanco-Bose, W., Jaworski, M., Offner, S., Dunant, C.F., Eshkind, L., Bockamp, E., et al. (2008). Hematopoietic stem cells reversibly switch from dormancy to self-renewal during homeostasis and repair. Cell *135*, 1118–1129.

Young, K.M., Fogarty, M., Kessaris, N., and Richardson, W.D. (2007). Subventricular zone stem cells are heterogeneous with respect to their embryonic origins and neurogenic fates in the adult olfactory bulb. J. Neurosci. *27*, 8286–8296.

Young, S.Z., Taylor, M.M., and Bordey, A. (2011). Neurotransmitters couple brain activity to subventricular zone neurogenesis. Eur. J. Neurosci. *33*, 1123–1132.

Zhuo, L., Sun, B., Zhang, C.L., Fine, A., Chiu, S.Y., and Messing, A. (1997). Live astrocytes visualized by green fluorescent protein in transgenic mice. Dev. Biol. *187*, 36–42.

Zimmerman, L., Parr, B., Lendahl, U., Cunningham, M., McKay, R., Gavin, B., Mann, J., Vassileva, G., and McMahon, A. (1994). Independent regulatory elements in the nestin gene direct transgene expression to neural stem cells or muscle precursors. Neuron *12*, 11–24.